

Spatially resolved Fourier holographic light scattering angular spectroscopy

Sergey A. Alexandrov, Timothy R. Hillman, and David D. Sampson

Optical and Biomedical Engineering Laboratory, School of Electrical, Electronic and Computer Engineering,
University of Western Australia, Crawley, Western Australia 6009, Australia

Received July 6, 2005; revised manuscript received September 9, 2005; accepted September 9, 2005

We show for what is the first time to our knowledge that digital Fourier holography can be used to record spatially resolved angular light scattering spectra from microscopically structured samples. This is achieved in one or a few digital image captures over large millimeter-scale fields of view. Such spectra are a sensitive measure of microscopic morphology, with wide applications in biological and medical imaging. We demonstrate good agreement between results of experiment and Mie theory for the angular scattering spectra of microspheres in water extracted from local regions within reconstructed 2×1 millimeter image sets.

© 2005 Optical Society of America

OCIS codes: 170.1650, 170.3880, 170.4580, 120.3890, 090.0090, 070.0070, 100.2000.

For many applications, particularly in biological microscopy and medical imaging, the significant areas of a sample are of millimeter or greater dimensions, but the spatial information of interest is on the microscopic scale. It remains laborious and time consuming to survey morphology (structure) by microscopic imaging, typically involving multiple tiled images of statistically significant populations of objects over large areas of samples. The ability to rapidly capture information that effectively characterizes the morphology on the microscopic scale over these large fields of view would be a useful advance. We seek to achieve this by exploiting the angular scattering spectrum of elastically scattered light, which is rapidly becoming recognized as a sensitive measure of microscopic morphology.¹ In this Letter we show for what is the first time to our knowledge that digital Fourier holography can be used to measure the angular spectrum of elastically scattered light at many spatial locations covering a large field of view based on a single capture or a few image captures.

There have been many recent attempts to use light scattering to deduce from biological samples morphological information connected to function or pathology.²⁻⁶ So-called light scattering spectroscopy began with the recording of the spectral distribution of scattering of a point,² which was followed by spectral imaging over large areas of samples.³ Combined with polarization gating^{3,5} to discriminate superficial from deeper layers in tissues, it has shown great promise in the detection of nuclear pleomorphism in epithelial tumours *in vivo*.^{3,5} More recently, the importance of angular distributions has begun to be appreciated in light scattering spectroscopy^{4,5,7} and in related approaches,^{1,6} including one based on optical Fourier filtering.⁶ Previously reported methods of recording angular scattering spectra involve either the capture of a single image point per measurement^{1,4,5} or have a small field of view and limited flexibility.⁶ We seek to improve on these methods through the use of digital holography, which has previously been successfully applied to microscopy.⁸ Our objective is to obtain the complex Fourier spectrum of light back-scattered from a sample (at low magnification over a

wide field of view³) by recording the interference pattern formed by the optical Fourier transform of the scattered wave^{6,9,10} and a reference wave. Digital Fourier filtering is then used to reconstruct spatially resolved angular scattering spectra. Uniquely, to our knowledge, we can produce such wide-field spectra from a single or a few image captures. They can be used to deduce morphological information at all points within the field of view, for example, in combination with Mie or other scattering theories to extract scatterer sizes and refractive index contrasts.^{4,5,11}

Let the complex representations in the recording plane of the Fourier transform of the scattered field and the reference field be $E_S(x,y)$ and $E_R(x,y) = A_R(x,y)\exp[-j2\pi(\alpha_Xx + \alpha_Yy)]$, respectively, where $A_R(x,y)$ is a slowly varying complex envelope and α_X , α_Y are spatial carrier frequencies imparted by the off-set angle of the reference wave with respect to the optical axis of the scattered wave. Then the recorded intensity distribution is

$$I(x,y) = |E_S|^2 + |A_R|^2 + E_S A_R^* \exp[j2\pi(\alpha_Xx + \alpha_Yy)] + E_S^* A_R \exp[-j2\pi(\alpha_Xx + \alpha_Yy)]. \quad (1)$$

When this intensity is inverse Fourier transformed, the first two terms yield zero-order autocorrelation and background images, centered at the origin. The third and fourth terms yield first-order twin images of the sample field and its (spatially inverted) complex conjugate, each translated in opposite directions due to the influence of the exponential carrier factors. If the first-order images are sufficiently spatially separated from the zero-order images, the squared magnitude of the entire reconstruction yields twin images of the scattered power from the sample. Otherwise, the first two terms can be removed by recording the sample and reference intensities separately and subtracting both from Eq. (1).

The complex angular spectrum of the scattered field depends on the scatterers' sizes and relative refractive indices with respect to the background medium.³ In the Fourier plane there is a one-to-one correspondence between spatial position and scattering angle.¹⁰ Therefore we perform spatial filtering of

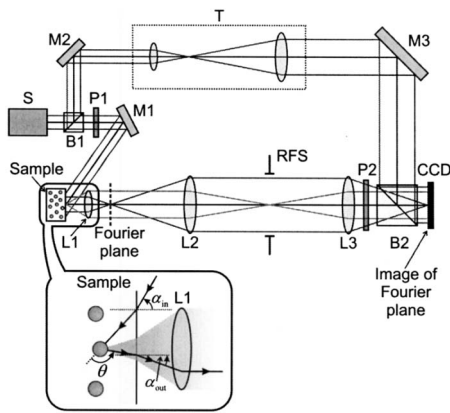


Fig. 1. Schematic diagram of the experimental setup. L1, L2, L3, lenses; M1, M2, M3, mirrors; B1, B2, beam splitters; P1, P2, polarizers; RFS, rectangular field stop; S, light source; T, telescopic system; CCD, CCD matrix sensor.

the Fourier hologram via a set of masks, which can be used to select (and weight) any given range of scattering angles. The subsequently reconstructed image is a spatially resolved plot of the power scattered in this solid angle range.

Figure 1 presents a schematic diagram of our experimental setup. A randomly polarized light beam from a He-Ne laser source S is split into reference and sample waves at beam splitter B1. A sample is placed at the object plane of a Fourier-transforming objective lens L1 ($f=15$ mm) and illuminated by a linearly polarized nearly plane wave. The optical Fourier spectrum of the backscattered light is formed in the back focal plane of objective lens L1. We chose a backscattering geometry to permit the future study of optically thick samples. A digital CCD matrix sensor (12 bit, 1392×1040 pixels, 7.6 mm \times 6.2 mm) is placed in a plane conjugate to this focal plane. The reference wave is expanded by using the telescopic system T and is directed to fill the CCD matrix (at an angle of 2.3° to the sample beam axis), forming the Fourier hologram. The value of the modulation spatial frequency imposed by the axial sample wave and the tilted reference wave is about 60 cycles/mm. The twin images are fully separated provided this value is greater than 30 cycles/mm (the CCD sensor array spacing is 215 pixels/mm). The angle of incidence α_{in} of the illumination wave is 69° (Fig. 1 inset). The plane of incidence is perpendicular to the plane of the CCD matrix, and the projection of the former plane onto the latter one is a diagonally oriented line. In the CCD plane, curves of constant scattering (polar) angle are therefore well approximated by lines perpendicular to this diagonal, within the limited size of the CCD matrix. The angular scattering range in air is $\Delta\alpha = \alpha_{out,max} - \alpha_{out,min} = 15^\circ$. The maximum and minimum values of the scattering angle θ within a sample of refractive index n_{med} are given by

$$\theta_{max/min} = \pi - \left[\arcsin\left(\frac{\sin \alpha_{in}}{n_{med}}\right) + \arcsin\left(\frac{\sin \alpha_{out,min/max}}{n_{med}}\right) \right]. \quad (2)$$

The values are shown in Fig. 2(a). The spatial filtering mask is a narrow slit corresponding to a scattering angle range (in the medium) of 1.2° (and the full range of azimuthal angles). It is digitally scanned in order to reconstruct images corresponding to each scattering angle. We may thus determine scattered power as a function of scattering angle for any sample region of interest by computing the total scattered power from this region in each reconstructed image.

Our samples comprised polystyrene spheres suspended in distilled water, with volume concentration of approximately 0.1%. A droplet was placed in a 10 mm \times 20 mm well on a microscope slide. A typical Fourier hologram of such a sample (sphere diameter 5.4 μ m), after subtraction of the reference and sample waves, is presented in Fig. 2(a), based on 400 ms exposures. The borders of two slit masks are shown overlaid on the hologram. Figure 2(b) shows a magnified portion of the modulation pattern. In Figs. 2(c) and 2(d) reconstructed filtered images are presented, corresponding to the two spatial filter locations. In order to clearly identify the twin first-order reconstructed images, the field of view has been restricted to a 2 mm \times 1 mm area by placing a rectangular field stop in the image plane. A direct comparison of the two reconstructions shows that the power distribution depends on the position of the spatial filter.

We applied the method to samples containing a mix of polystyrene spheres of two different diameters, 5.4 and 11.4 μ m (with respective standard deviations 0.14 and 0.21 μ m). Figure 3 (top) shows the reconstructed image of the sample. For two selected locations on the reconstructed image, the angular power dependence was obtained by using the set of

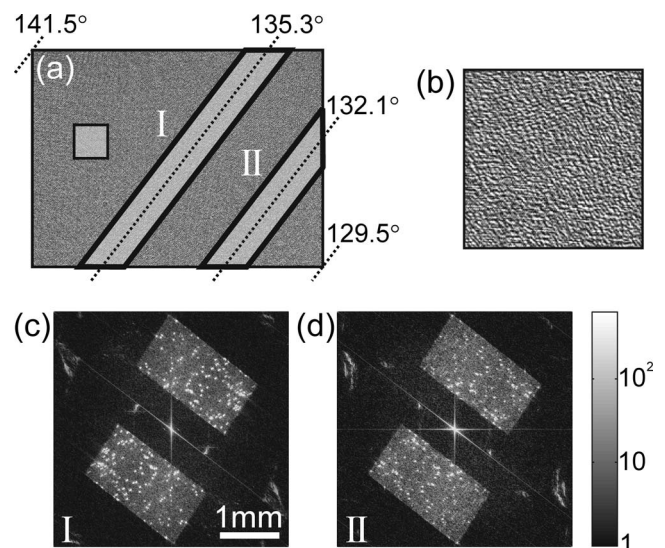


Fig. 2. (a) Recorded Fourier spectrum of the sample containing microspheres, diameter 5.4 μ m, with two positions of the spatial filter shown. Each dotted line corresponds to a given scattering angle. The highlighted square is magnified in (b). (c), (d) Reconstructed filtered images for positions (I), (II) of the spatial filter, respectively, displayed with a logarithmic gray scale. The images are scaled by the inverse area of the filter.

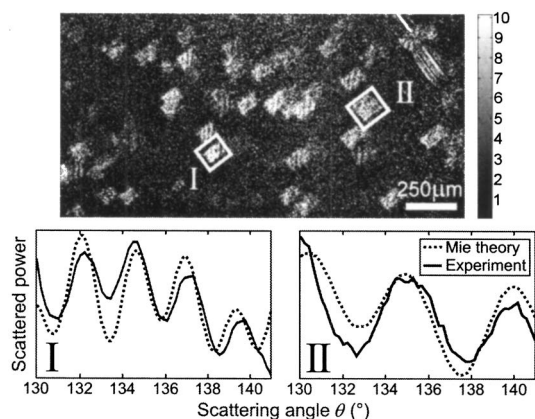


Fig. 3. Reconstructed image of a sample containing microspheres of two different diameters, 5.4 and 11.4 μm , suspended in distilled water, displayed with a linear gray scale. For regions I and II the angular dependence of the scattered power is plotted against the theoretical predictions of Mie theory (with the optimum fit corresponding to diameters 5.2 and 11.2 μm , respectively).

reconstructed images over the full range of angles. The corresponding angular-dependent scattering plots (overlaid with the results of Mie theory) are presented in Fig. 3. The agreement between experiment and theory is good, demonstrating the ability of our approach to discriminate scatterer size in each local area of the sample.

The large field of view demonstrated here is possible because of the encoding of microscopic information in the angular scattering spectrum. The microspheres are too small for their size to be accurately determined directly from the reconstructed image, in which the pixel size is approximately 3 μm . Thus, we have shown that high spatial resolution is not necessary to characterize the microstructure of the sample. Fundamentally, the spatial resolution of our approach is traded off with angular resolution. Decreasing the range of solid angles contributing to the image, by decreasing the mask area, degrades the spatial resolution of the reconstructed image. Our choice of a rectangular $1.2^\circ \times 8.9^\circ$ (maximum) mask yields an impulse response width (main lobe) of 50 $\mu\text{m} \times 6 \mu\text{m}$. It also means that the angle-resolved scattered power curves are effectively convolved with a rectangular function of width 1.2° . The choice of angular and spatial resolution will be determined by the needs of a given application.

The implementation reported here does not perform optical sectioning, but polarization sensitivity³⁻⁵ can be incorporated into our setup by rotating polarizer P2 relative to P1, enabling partial discrimination of multiply scattered light arising from deeper locations in a thick sample. Depth sectioning by coherence gating^{7,11,12} should also be possible, since its use in depth-resolved holography has already been reported.¹³

The good agreement with Mie theory shown in Fig. 3 suggests that an inversion procedure to extract scatterer size and refractive index contrast should be

feasible. In biological samples, such a process may be limited by the complexity of the angular scattering spectra and the lack of a suitable model.⁴ In such cases, it may still be useful to map spatial variations in angular scattering spectra, for example, to enable the calculation of the fractal dimensions of tissue microarchitecture.^{5,11} It may also be possible to measure azimuthal scattering patterns or to incorporate spectral dependence by using a light source with several wavelengths.

The ability to record spatially resolved angular scattering spectra with one or a few image captures opens up many possibilities for the efficient and potentially dynamic study of microstructure. In biology and medicine, this includes the efficient high-throughput characterization of processes such as mitosis and apoptosis⁶ through the microscopic observation of cells; the study of tissue structures, for example, the assessment of muscle damage and regeneration in muscular dystrophy; and imaging tissues, for example, the *in vivo* detection of dysplasia.^{3,5}

S. A. Alexandrov is supported by the Raine Medical Research Foundation. We acknowledge contributions to the work presented here by Abbey Trewenack and Guido Kudielka and are grateful for early discussions with Steve Jacques. S. A. Alexandrov's e-mail address is sergey@ee.uwa.edu.au.

References

1. J. C. Ramella-Roman, P. R. Bargo, S. A. Prahl, and S. L. Jacques, *IEEE J. Sel. Top. Quantum Electron.* **9**, 301 (2003).
2. V. Backman, M. B. Wallace, L. T. Perelman, J. T. Arendt, R. Gurjar, M. G. Müller, Q. Zhang, G. Zonios, E. Kline, T. McGillican, S. Shapshay, T. Valdez, K. Badizadegan, J. M. Crawford, M. Fitzmaurice, S. Kabani, H. S. Levin, M. Seiler, R. R. Dasari, I. Itzkan, J. Van Dam, and M. S. Feld, *Nature* **406**, 35 (2000).
3. R. S. Gurjar, V. Backman, L. T. Perelman, I. Georgakoudi, K. Badizadegan, I. Itzkan, R. R. Dasari, and M. S. Feld, *Nat. Med.* **7**, 1245 (2001).
4. J. R. Mourant, T. M. Johnson, S. Carpenter, A. Guerra, T. Aida, and J. P. Freyer, *J. Biomed. Opt.* **7**, 378 (2002).
5. Y. L. Kim, Y. Liu, R. K. Wali, H. K. Roy, M. J. Goldberg, A. K. Kromin, K. Chen, and V. Backman, *IEEE J. Sel. Top. Quantum Electron.* **9**, 243 (2003).
6. N. N. Boustany, S. C. Kuo, and N. V. Thakor, *Opt. Lett.* **26**, 1063 (2001).
7. J. W. Pyhtila and A. Wax, *Opt. Express* **12**, 6178 (2004).
8. E. Cuche, F. Bevilacqua, and C. Depeursinge, *Opt. Lett.* **24**, 291 (1999).
9. G. Popescu, L. P. Deflores, J. C. Vaughan, K. Badizadegan, H. Iwai, R. R. Dasari, and M. S. Feld, *Opt. Lett.* **29**, 2503 (2004).
10. M. T. Valentine, A. K. Popp, D. A. Weitz, and P. D. Kaplan, *Opt. Lett.* **26**, 890 (2001).
11. A. Wax, C. Yang, V. Backman, K. Badizadegan, C. W. Boone, R. R. Dasari, and M. S. Feld, *Biophys. J.* **82**, 2256 (2002).
12. R. N. Graf and A. Wax, *Opt. Express* **13**, 4693 (2005).
13. M. Tziraki, R. Jones, P. M. W. French, M. R. Melloch, and D. D. Nolte, *Appl. Phys. B* **70**, 151 (2000).